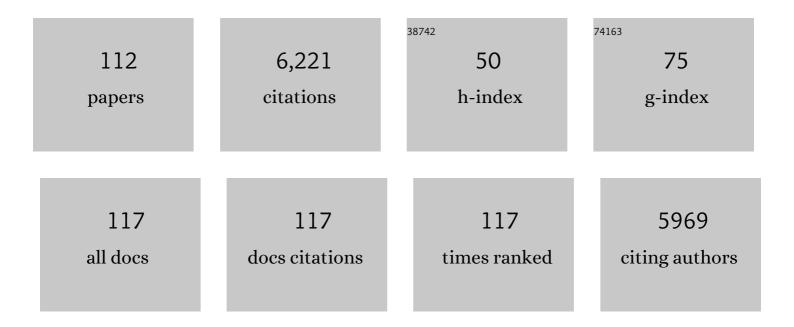
## Jeffrey Catalano

List of Publications by Year in descending order

Source: https://exaly.com/author-pdf/2065559/publications.pdf Version: 2024-02-01



#	Article	IF	CITATIONS
1	Consistent controls on trace metal micronutrient speciation in wetland soils and stream sediments. Geochimica Et Cosmochimica Acta, 2022, 317, 234-254.	3.9	8
2	Rates and Products of Iron Oxidation by Chlorate at Low Temperatures (0 to 25 °C) and Implications for Mars Geochemistry. ACS Earth and Space Chemistry, 2022, 6, 250-260.	2.7	6
3	Canyon Wall and Floor Debris Deposits in Aeolis Mons, Mars. Journal of Geophysical Research E: Planets, 2022, 127, .	3.6	2
4	Impact of Zn substitution on Fe(II)-induced ferrihydrite transformation pathways. Geochimica Et Cosmochimica Acta, 2022, 320, 143-160.	3.9	15
5	Impact of dissolved oxygen and pH on the removal of selenium from water by iron electrocoagulation. Water Research, 2022, 213, 118159.	11.3	17
6	Reduction of U(VI) on Chemically Reduced Montmorillonite and Surface Complexation Modeling of Adsorbed U(IV). Environmental Science & Technology, 2022, 56, 4111-4120.	10.0	19
7	First-principles characterisation and comparison of clean, hydrated, and defect α-Al <sub>2</sub> O <sub>3</sub> and α-Fe <sub>2</sub> O <sub>3</sub> (110) surfaces. Molecular Simulation, 2022, 48, 247-263.	2.0	4
8	Dynamic Responses of Trace Metal Bioaccessibility to Fluctuating Redox Conditions in Wetland Soils and Stream Sediments. ACS Earth and Space Chemistry, 2022, 6, 1331-1344.	2.7	7
9	Copper availability governs nitrous oxide accumulation in wetland soils and stream sediments. Geochimica Et Cosmochimica Acta, 2022, 327, 96-115.	3.9	5
10	Redox-Driven Recrystallization of PbO <sub>2</sub> . Environmental Science & Technology, 2022, 56, 7864-7872.	10.0	4
11	Resolving Configurational Disorder for Impurities in a Low-Entropy Phase. Journal of Physical Chemistry Letters, 2021, 12, 5689-5694.	4.6	6
12	Effects of Cu(II) and Zn(II) on PbO <sub>2</sub> Reductive Dissolution under Drinking Water Conditions: Short-term Inhibition and Long-term Enhancement. Environmental Science & Technology, 2021, 55, 14397-14406.	10.0	8
13	The future low-temperature geochemical data-scape as envisioned by the U.S. geochemical community. Computers and Geosciences, 2021, 157, 104933.	4.2	3
14	Effects of Phosphate Competition on Arsenate Binding to Aluminum Hydroxide Surfaces. ACS Earth and Space Chemistry, 2021, 5, 3140-3149.	2.7	1
15	Density Functional Theory and Thermodynamics Modeling of Inner-Sphere Oxyanion Adsorption on the Hydroxylated α-Al <sub>2</sub> O <sub>3</sub> (001) Surface. Langmuir, 2020, 36, 13166-13180.	3.5	19
16	Evidence for a Diagenetic Origin of Vera Rubin Ridge, Gale Crater, Mars: Summary and Synthesis of <i>Curiosity</i> 's Exploration Campaign. Journal of Geophysical Research E: Planets, 2020, 125, e2020JE006527.	3.6	69
17	Capacity of Chlorate to Oxidize Ferrous Iron: Implications for Iron Oxide Formation on Mars. Minerals (Basel, Switzerland), 2020, 10, 729.	2.0	15
18	The quench control of water estimates in convergent margin magmas. American Mineralogist, 2019, 104–936-948	1.9	26

#	Article	IF	CITATIONS
19	Chlorate as a Potential Oxidant on Mars: Rates and Products of Dissolved Fe(II) Oxidation. Journal of Geophysical Research E: Planets, 2019, 124, 2893-2916.	3.6	33
20	The source of sulfate in brachiopod calcite: Insights from $\hat{I}_4$ -XRF imaging and XANES spectroscopy. Chemical Geology, 2019, 529, 119328.	3.3	10
21	Association of Defects and Zinc in Hematite. Environmental Science & Technology, 2019, 53, 13687-13694.	10.0	20
22	Emerging investigator series: linking chemical transformations of silver and silver nanoparticles in the extracellular and intracellular environments to their bio-reactivity. Environmental Science: Nano, 2019, 6, 2948-2957.	4.3	7
23	Insights into past ocean proxies from micron-scale mapping of sulfur species in carbonates. Geology, 2019, 47, 833-837.	4.4	12
24	Understanding the Roles of Dissolution and Diffusion in Cr(OH) <sub>3</sub> Oxidation by Î-MnO <sub>2</sub> . ACS Earth and Space Chemistry, 2019, 3, 357-365.	2.7	33
25	Depositional and diagenetic constraints on the abundance and spatial variability of carbonate-associated sulfate. Chemical Geology, 2019, 523, 59-72.	3.3	23
26	Reductive transformations of layered manganese oxides by small organic acids and the fate of trace metals. Geochimica Et Cosmochimica Acta, 2019, 250, 149-172.	3.9	41
27	Comparative response of interfacial water structure to pH variations and arsenate adsorption on corundum (0 1 2) and (0 0 1) surfaces. Geochimica Et Cosmochimica Acta, 2019, 246, 406-418.	3.9	7
28	The surface chemistry of sapphire-c: A literature review and a study on various factors influencing its IEP. Advances in Colloid and Interface Science, 2018, 251, 1-25.	14.7	25
29	Spectral and stratigraphic mapping of hydrated minerals associated with interior layered deposits near the southern wall of Melas Chasma, Mars. Icarus, 2018, 302, 62-79.	2.5	14
30	Retrieval of Compositional Endâ€Members From Mars Exploration Rover Opportunity Observations in a Soilâ€Filled Fracture in Marathon Valley, Endeavour Crater Rim. Journal of Geophysical Research E: Planets, 2018, 123, 278-290.	3.6	11
31	Insights on the Alumina–Water Interface Structure by Direct Comparison of Density Functional Simulations with X-ray Reflectivity. Journal of Physical Chemistry C, 2018, 122, 26934-26944.	3.1	19
32	Influence of Oxalate on Ni Fate during Fe(II)-Catalyzed Recrystallization of Hematite and Goethite. Environmental Science & Technology, 2018, 52, 6920-6927.	10.0	16
33	Martian Habitability as Inferred From Landed Mission Observations. , 2018, , 77-126.		5
34	Effects of Ionic Strength on Arsenate Adsorption at Aluminum Hydroxide–Water Interfaces. Soil Systems, 2018, 2, 1.	2.6	22
35	Response of interfacial water to arsenate adsorption on corundum (0â€ <sup>-</sup> 0â€ <sup>-</sup> 1) surfaces: Effects of pH and adsorbate surface coverage. Geochimica Et Cosmochimica Acta, 2018, 239, 198-212.	3.9	16
36	Impact of Mn(II)-Manganese Oxide Reactions on Ni and Zn Speciation. Environmental Science & Technology, 2017, 51, 3187-3196.	10.0	37

#	Article	IF	CITATIONS
37	Effect of Humic Acid on the Removal of Chromium(VI) and the Production of Solids in Iron Electrocoagulation. Environmental Science & Technology, 2017, 51, 6308-6318.	10.0	95
38	Oxalate-Promoted Trace Metal Release from Crystalline Iron Oxides under Aerobic Conditions. Environmental Science and Technology Letters, 2017, 4, 311-315.	8.7	18
39	Engineering Nanoscale Iron Oxides for Uranyl Sorption and Separation: Optimization of Particle Core Size and Bilayer Surface Coatings. ACS Applied Materials & Interfaces, 2017, 9, 13163-13172.	8.0	44
40	Rates of Cr(VI) Generation from Cr <sub><i>x</i></sub> Fe <sub>1–<i>x</i></sub> (OH) <sub>3</sub> Solids upon Reaction with Manganese Oxide. Environmental Science & Technology, 2017, 51, 12416-12423.	10.0	78
41	Competitive and Cooperative Effects during Nickel Adsorption to Iron Oxides in the Presence of Oxalate. Environmental Science & amp; Technology, 2017, 51, 9792-9799.	10.0	46
42	Oxidative Alteration of Ferrous Smectites and Implications for the Redox Evolution of Early Mars. Journal of Geophysical Research E: Planets, 2017, 122, 2469-2488.	3.6	28
43	Phosphate-Induced Immobilization of Uranium in Hanford Sediments. Environmental Science & Technology, 2016, 50, 13486-13494.	10.0	37
44	High concentrations of manganese and sulfur in deposits on Murray Ridge, Endeavour Crater, Mars. American Mineralogist, 2016, 101, 1389-1405.	1.9	55
45	Impacts of Surface Site Coordination on Arsenate Adsorption: Macroscopic Uptake and Binding Mechanisms on Aluminum Hydroxide Surfaces. Langmuir, 2016, 32, 13261-13269.	3.5	17
46	Dynamics of Chromium(VI) Removal from Drinking Water by Iron Electrocoagulation. Environmental Science & Technology, 2016, 50, 13502-13510.	10.0	107
47	Implications for the aqueous history of southwest Melas Chasma, Mars as revealed by interbedded hydrated sulfate and Fe/Mg-smectite deposits. Icarus, 2016, 271, 283-291.	2.5	10
48	Effect of phosphate on U(VI) sorption to montmorillonite: Ternary complexation and precipitation barriers. Geochimica Et Cosmochimica Acta, 2016, 175, 86-99.	3.9	68
49	Structural response of phyllomanganates to wet aging and aqueous Mn(II). Geochimica Et Cosmochimica Acta, 2016, 192, 220-234.	3.9	60
50	Engineered superparamagnetic iron oxide nanoparticles for ultra-enhanced uranium separation and sensing. Journal of Materials Chemistry A, 2016, 4, 15022-15029.	10.3	24
51	Smectite deposits in Marathon Valley, Endeavour Crater, Mars, identified using CRISM hyperspectral reflectance data. Geophysical Research Letters, 2016, 43, 4885-4892.	4.0	39
52	Effect of Reaction Pathway on the Extent and Mechanism of Uranium(VI) Immobilization with Calcium and Phosphate. Environmental Science & amp; Technology, 2016, 50, 3128-3136.	10.0	52
53	Mars Reconnaissance Orbiter and Opportunity observations of the Burns formation: Crater hopping at Meridiani Planum. Journal of Geophysical Research E: Planets, 2015, 120, 429-451.	3.6	30
54	Synthesis and structural characterization of ferrous trioctahedral smectites: Implications for clay mineral genesis and detectability on Mars. Journal of Geophysical Research E: Planets, 2015, 120, 1119-1140.	3.6	50

#	Article	IF	CITATIONS
55	Effect of phosphate and sulfate on Ni repartitioning during Fe(II)-catalyzed Fe(III) oxide mineral recrystallization. Geochimica Et Cosmochimica Acta, 2015, 165, 62-74.	3.9	13
56	Interaction of Fe(II) with phosphate and sulfate on iron oxide surfaces. Geochimica Et Cosmochimica Acta, 2015, 158, 130-146.	3.9	84
57	Transport of U(VI) through sediments amended with phosphate to induce in situ uranium immobilization. Water Research, 2015, 69, 307-317.	11.3	43
58	Engineered manganese oxide nanocrystals for enhanced uranyl sorption and separation. Environmental Science: Nano, 2015, 2, 500-508.	4.3	43
59	Ancient Aqueous Environments at Endeavour Crater, Mars. Science, 2014, 343, 1248097.	12.6	176
60	Effect of co-solutes on the products and solubility of uranium(VI) precipitated with phosphate. Chemical Geology, 2014, 364, 66-75.	3.3	75
61	A hematite-bearing layer in Gale Crater, Mars: Mapping and implications for past aqueous conditions. Geology, 2013, 41, 1103-1106.	4.4	113
62	Adsorption of Uranium(VI) to Manganese Oxides: X-ray Absorption Spectroscopy and Surface Complexation Modeling. Environmental Science & Technology, 2013, 47, 850-858.	10.0	187
63	Thermodynamic and mass balance constraints on ironâ€bearing phyllosilicate formation and alteration pathways on early Mars. Journal of Geophysical Research E: Planets, 2013, 118, 2124-2136.	3.6	49
64	Fate of Metals in Fly Ash During Aging in Laboratory-Scale Ash Impoundments. Environmental Engineering Science, 2012, 29, 1085-1091.	1.6	4
65	Characteristics and Outcomes of Sentinel Node–Positive Breast Cancer Patients after Total Mastectomy without Axillary-Specific Treatment. Annals of Surgical Oncology, 2012, 19, 3762-3770.	1.5	56
66	Inhibition of Trace Element Release During Fe(II)-Activated Recrystallization of Al-, Cr-, and Sn-Substituted Goethite and Hematite. Environmental Science & Technology, 2012, 46, 10031-10039.	10.0	61
67	Metal Release and Speciation Changes during Wet Aging of Coal Fly Ashes. Environmental Science & Technology, 2012, 46, 11804-11812.	10.0	46
68	Distribution and speciation of trace elements in iron and manganese oxide cave deposits. Geochimica Et Cosmochimica Acta, 2012, 91, 240-253.	3.9	57
69	Fe(II)-Mediated Reduction and Repartitioning of Structurally Incorporated Cu, Co, and Mn in Iron Oxides. Environmental Science & Technology, 2012, 46, 11070-11077.	10.0	63
70	Lambert albedo retrieval and analyses over Aram Chaos from OMEGA hyperspectral imaging data. Journal of Geophysical Research, 2012, 117, .	3.3	14
71	Controls on Fe(II)-Activated Trace Element Release from Goethite and Hematite. Environmental Science & Technology, 2012, 46, 1519-1526.	10.0	101
72	Molecular-Scale Structure of Uranium(VI) Immobilized with Goethite and Phosphate. Environmental Science & Technology, 2012, 46, 6594-6603.	10.0	93

#	Article	IF	CITATIONS
73	Radiation field design and regional control in sentinel lymph nodeâ€positive breast cancer patients with omission of axillary dissection. Cancer, 2012, 118, 1994-2003.	4.1	25
74	Speciation of Selenium, Arsenic, and Zinc in Class C Fly Ash. Energy & Fuels, 2011, 25, 2980-2987.	5.1	63
75	Composition and structure of nanocrystalline Fe and Mn oxide cave deposits: Implications for trace element mobility in karst systems. Chemical Geology, 2011, 284, 82-96.	3.3	78
76	Isotopic fractionation of Cu in plants. Chemical Geology, 2011, , .	3.3	18
77	Weak interfacial water ordering on isostructural hematite and corundum (001) surfaces. Geochimica Et Cosmochimica Acta, 2011, 75, 2062-2071.	3.9	100
78	Effect of Aqueous Fe(II) on Arsenate Sorption on Goethite and Hematite. Environmental Science & Technology, 2011, 45, 8826-8833.	10.0	74
79	Trace element cycling through iron oxide minerals during redox-driven dynamic recrystallization. Geology, 2011, 39, 1083-1086.	4.4	97
80	Concentrated perchlorate at the Mars Phoenix landing site: Evidence for thin film liquid water on Mars. Geophysical Research Letters, 2010, 37, .	4.0	92
81	Spirit Mars Rover Mission: Overview and selected results from the northern Home Plate Winter Haven to the side of Scamander crater. Journal of Geophysical Research, 2010, 115, .	3.3	127
82	Relaxations and Interfacial Water Ordering at the Corundum (110) Surface. Journal of Physical Chemistry C, 2010, 114, 6624-6630.	3.1	40
83	Structure and oxidation state of hematite surfaces reacted with aqueous Fe(II) at acidic and neutral pH. Geochimica Et Cosmochimica Acta, 2010, 74, 1498-1512.	3.9	76
84	Probing interfacial reactions with X-ray reflectivity and X-ray reflection interface microscopy: Influence of NaCl on the dissolution of orthoclase at pOH 2 and 85°C. Geochimica Et Cosmochimica Acta, 2010, 74, 3396-3411.	3.9	14
85	Mineralization of contaminant uranium and leach rates in sediments from Hanford, Washington. Applied Geochemistry, 2010, 25, 97-104.	3.0	6
86	Water ordering and surface relaxations at the hematite (110)–water interface. Geochimica Et Cosmochimica Acta, 2009, 73, 2242-2251.	3.9	58
87	Nanoscale Size Effects on Uranium(VI) Adsorption to Hematite. Environmental Science & Technology, 2009, 43, 1373-1378.	10.0	133
88	Simultaneous inner- and outer-sphere arsenate adsorption on corundum and hematite. Geochimica Et Cosmochimica Acta, 2008, 72, 1986-2004.	3.9	220
89	Sequestration of Sr(II) by calcium oxalate—A batch uptake study and EXAFS analysis of model compounds and reaction products. Geochimica Et Cosmochimica Acta, 2008, 72, 5055-5069.	3.9	18
90	Bridging arsenate surface complexes on the hematite (012) surface. Geochimica Et Cosmochimica Acta, 2007, 71, 1883-1897.	3.9	103

#	Article	IF	CITATIONS
91	Interfacial water structure on the (012) surface of hematite: Ordering and reactivity in comparison with corundum. Geochimica Et Cosmochimica Acta, 2007, 71, 5313-5324.	3.9	79
92	Surface diffraction study of the hydrated hematite surface. Surface Science, 2007, 601, 460-474.	1.9	97
93	Hydrated α-Fe2O3 surface structure: Role of surface preparation. Surface Science, 2007, 601, L59-L64.	1.9	57
94	Changes in Uranium Speciation through a Depth Sequence of Contaminated Hanford Sediments. Environmental Science & Technology, 2006, 40, 2517-2524.	10.0	135
95	Termination and Water Adsorption at the α-Al2O3(012)â^'Aqueous Solution Interface. Langmuir, 2006, 22, 4668-4673.	3.5	99
96	Structure of hydrated Zn2+ at the rutile TiO2 (110)-aqueous solution interface: Comparison of X-ray standing wave, X-ray absorption spectroscopy, and density functional theory results. Geochimica Et Cosmochimica Acta, 2006, 70, 4039-4056.	3.9	52
97	On the use of CCD area detectors for high-resolution specular X-ray reflectivity. Journal of Synchrotron Radiation, 2006, 13, 293-303.	2.4	47
98	Inner-sphere adsorption geometry of Se(IV) at the hematite (100)–water interface. Journal of Colloid and Interface Science, 2006, 297, 665-671.	9.4	74
99	Experimental determination of UO2(cr) dissolution kinetics: Effects of solution saturation state and pH. Journal of Nuclear Materials, 2005, 345, 206-218.	2.7	68
100	Surface complexation studied via combined grazing-incidence EXAFS and surface diffraction: arsenate on hematite (0001) and (10–12). Analytical and Bioanalytical Chemistry, 2005, 383, 12-27.	3.7	66
101	Synthesis and characterization of sodium meta-autunite, Na[UO2PO4]·3H2O. Radiochimica Acta, 2005, 93, .	1.2	22
102	Fluorescence spectroscopy of U(VI)-silicates and U(VI)-contaminated Hanford sediment. Geochimica Et Cosmochimica Acta, 2005, 69, 1391-1403.	3.9	136
103	Uranyl adsorption onto montmorillonite: Evaluation of binding sites and carbonate complexation. Geochimica Et Cosmochimica Acta, 2005, 69, 2995-3005.	3.9	248
104	CTR diffraction and grazing-incidence EXAFS study of U(VI) adsorption onto α-Al2O3 and α-Fe2O3 (11̄02) surfaces. Geochimica Et Cosmochimica Acta, 2005, 69, 3555-3572.	3.9	84
105	Sorption and precipitation of Co(II) in Hanford sediments and alkaline aluminate solutions. Applied Geochemistry, 2005, 20, 193-205.	3.0	19
106	Analysis of uranyl-bearing phases by EXAFS spectroscopy: Interferences, multiple scattering, accuracy of structural parameters, and spectral differences. American Mineralogist, 2004, 89, 1004-1021.	1.9	90
107	Structure and reactivity of the hydrated hematite (0001) surface. Surface Science, 2004, 573, 204-224.	1.9	279
108	Spectroscopic and Diffraction Study of Uranium Speciation in Contaminated Vadose Zone Sediments from the Hanford Site, Washington State. Environmental Science & Technology, 2004, 38, 2822-2828.	10.0	96

#	Article	IF	CITATIONS
109	Chromium speciation and mobility in a high level nuclear waste vadose zone plume. Geochimica Et Cosmochimica Acta, 2004, 68, 13-30.	3.9	103
110	Enthalpies of formation of U-, Th-, Ce-brannerite: implications for plutonium immobilization. Journal of Nuclear Materials, 2003, 320, 231-244.	2.7	56
111	Molecular beam epitaxial growth and properties of CoFe2O4 on MgO(001). Journal of Magnetism and Magnetic Materials, 2002, 246, 124-139.	2.3	134
112	Enthalpies of formation of Ce-pyrochlore, Ca0.93Ce1.00Ti2.035O7.00, U-pyrochlore, Ca1.46U4+0.23U6+0.46Ti1.85O7.00 and Gd-pyrochlore, Gd2Ti2O7: three materials relevant to the proposed waste form for excess weapons plutonium. Journal of Nuclear Materials, 2002, 303, 226-239.	2.7	84